PAPER • **OPEN ACCESS**

Fluorophore photostability and saturation in the hotspot of DNA origami nanoantennas

To cite this article: Lennart Grabenhorst *et al* 2020 *Methods Appl. Fluoresc.* **8** 024003

Methods and Applications in Fluorescence

PAPER

Fluorophore photostability and saturation in the hotspot of DNA origami nanoantennas

Lennart Grabenhorst[1,3], **Kateryna Trofymchuk**[1,2,3], **Florian Steiner**[1], **Viktorija Glembockyte**[1,4] and **Philip Tinnefeld**[1,4]

[1] Department of Chemistry and Center for NanoScience, Ludwig-Maximilians-Universität München, Butenandtstr. 5-13, 81377 München, Germany
[2] Institute for Physical and Theoretical Chemistry—NanoBioScience and Braunschweig Integrated Centre of Systems Biology (BRICS), Technische Universität Braunschweig, Braunschweig, Germany
[3] These authors contributed equally.
[4] Author to whom any correspondence should be addressed.

E-mail: philip.tinnefeld@cup.lmu.de **and** viktorija.glembockyte@cup.lmu.de

Keywords: DNA nanotechnology, fluorescence microscopy, photostability, nanophotonics, plasmonics

Supplementary material for this article is available online

OPEN ACCESS

RECEIVED
30 August 2019

REVISED
18 December 2019

ACCEPTED FOR PUBLICATION
13 January 2020

PUBLISHED
5 February 2020

Abstract

Fluorescent dyes used for single-molecule spectroscopy can undergo millions of excitation-emission cycles before photobleaching. Due to the upconcentration of light in a plasmonic hotspot, the conditions for fluorescent dyes are even more demanding in DNA origami nanoantennas. Here, we briefly review the current state of fluorophore stabilization for single-molecule imaging and reveal additional factors relevant in the context of plasmonic fluorescence enhancement. We show that despite the improved photostability of single-molecule fluorophores by DNA origami nanoantennas, their performance in the intense electric fields in plasmonic hotspots is still limited by the underlying photophysical processes, such as formation of dim states and photoisomerization. These photophysical processes limit the photon count rates, increase heterogeneity and aggravate quantification of fluorescence enhancement factors. These factors also reduce the time resolution that can be achieved in biophysical single-molecule experiments. Finally, we show how the photophysics of a DNA hairpin assay with a fluorophore-quencher pair can be influenced by plasmonic DNA origami nanoantennas leading to implications for their use in fluorescence-based diagnostic assays. Especially, we show that such assays can produce false positive results by premature photobleaching of the dark quencher.

Introduction

For many years, researchers have been pushing organic fluorophores to their limits—simply because the fluorophore is the main bottleneck in most experiments involving fluorescence [1]. Photobleaching processes limit both the observation time of the molecule and the achievable time resolution of an experiment. This is especially relevant for observables that cannot be obtained from quasi-ensemble measurements such as nanosecond-fluorescence correlation spectroscopy (ns-FCS) [2] and require true single-molecule data, e.g. the observation of transition paths in conformational dynamics of biomolecules [3]. Furthermore, preliminary bleaching of fluorophores and quenchers can also influence the reliability of fluorescence-based diagnostic assays. This push for more photons and stable fluorescence signal has led to new mechanistic insights of fluorophore photobleaching pathways as well as to the discovery of a plethora of suitable photostabilization strategies [1, 4–8]. In this paper, we briefly review the processes governing photostability and strategies to increase photostability with a focus on quenching intermediate states on the photobleaching pathway. We then place this discussion into the context of fluorophores next to plasmonic nanostructures. Based on our experimental data of photophysical effects and photostabilization in optical nanoantennas we reason that dim states of fluorophores are strikingly reducing the linear excitation intensity-dependent brightness of fluorophores and increase heterogeneity of fluorescence enhancement

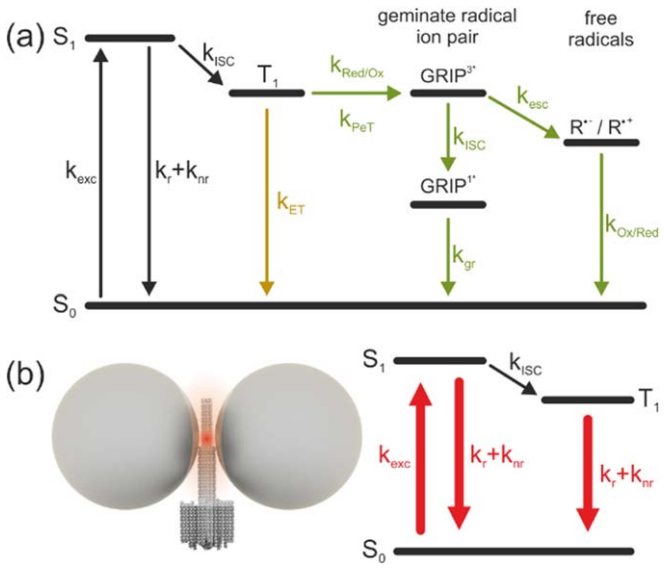

Scheme 1. Illustration of different mechanistic approaches used to improve the photostability of the fluorophores in single-molecule fluorescence applications. (a) Established photostabilization strategies: quenching the reactive fluorophore intermediates (triplet excited and radical species) via photophysical (energy transfer, orange) and photochemical (P*e*T, green) pathways. (b) Plasmonic nanostructures: photostability is improved by acceleration of the radiative decay rate depicted by bold arrows and minimizing the time the fluorophore spends in higher excited (reactive) states. Left: sketch of a DNA origami optical nanoantenna; fluorophore positioned in the hotspot between two metal nanoparticles. Right: simplified Jablonski diagram highlighting the photophysical rates (red) accelerated by nanoantennas. Here k_{exc} is the excitation rate, k_r the radiative and and k_{nr} non-radiative rate, k_{isc} the intersystem crossing rate, $k_{Red/Ox}$ the reduction (or oxidation) rate, k_{esc} the escape rate for the geminate radical ion pair (GRIP) to the free radical ($R\cdot^{+}/R\cdot^{-}$), and k_{gr} is the geminate recombination rate to the ground state.

values. In addition, the increased excitation fields and nonlinear bleaching pathways lead to photodestruction of fluorescence quencher molecules potentially leading to false positive results in basic assays of molecular diagnostics.

The total number of photons that can be detected from a given fluorophore is limited by its intrinsic photophysics and photochemistry [1, 9, 10]. An ideal fluorophore would cycle between its ground (S_0) and singlet excited (S_1) states emitting photons and reporting on the position or the state of the fluorescently labelled molecule (scheme 1(a)). At the high excitation rates required for single-molecule detection other photophysical processes come into play [11–13]. Intersystem crossing to the triplet excited state (T_1) can lead to long-lived and reactive triplet species. Furthermore, reduction or (photo)oxidation of the singlet or triplet excited state can lead to the formation of even longer-lived dark radical intermediates. While the triplet excited state is efficiently quenched by molecular oxygen, it leads to the generation of singlet oxygen as well as other reactive oxygen species capable of further accelerating the photobleaching reactions. Hence, established photostabilization approaches used to address these instabilities rely on combining the removal of oxygen (often via the use of enzymatic oxygen scavengers) with the addition of photostabilization additives that act as quenchers of reactive triplet and radical intermediates [8, 14].

With respect to triplet excited state quenchers, two mechanistically distinct approaches have been utilized (scheme 1(a)). On the one hand, triplet excited states can be quenched via a photophysical pathway (i.e. energy transfer) by photostabilizers like cyclooctatetraene (COT) [8, 14] or Ni^{2+} ions [7, 15, 16]. On the other hand, triplet excited states can also be quenched via photoinduced electron transfer (P*e*T) with a reducing (e.g. ascorbic acid [5], Trolox [4, 6, 8], β-mercaptoethanol (β-ME) [6]) or an oxidizing agent (e.g. methyl viologen [5], Trolox quinone [4], 4-nitrobenzyl alcohol) which results in the formation of a radical anion or a radical cation, respectively. The resulting radical intermediates are rescued by the simultaneous use of both reducing and oxidizing agents—an approach that is known as reducing and oxidizing system (ROXS) [5]. The formation of long-lived radical intermediates and requirement of the complementary redox partner can be avoided if the P*e*T is followed by fast back electron transfer [17]. This requires a redox partner capable of assisting an intersystem crossing in the triplet geminate radical ion pair that is formed following the P*e*T step (scheme 1(a)) [18]. While these solution-based photostabilization approaches have significantly advanced single-molecule fluorescence studies by allowing to extend the experiments from few seconds to tens of minutes and providing photon budgets reaching millions [5, 7], one always has to keep in mind the potential influence of the photostabilizers on the biological system under investigation. One strategy that has been realized over the last decade to address this issue relies on direct coupling of photostabilizers with the fluorophores to

obtain 'self-healing' dyes [19]. Several small molecules have been conjugated or proximally linked to different single-molecule dyes that include COT [20–24], Trolox [20–24], 4-nitrobenzyl alcohol (NBA) [20], nitrophenylalanine (NPA) [21, 22, 25, 26], or a *tris*NTA moiety containing three Ni^{2+} ions [16].

The conventional approaches revolve around salvaging the pristine, fluorescent state from its reactive and non-emissive triplet or radical forms by supplying the appropriate reaction partner. Recently, another strategy for photostabilization has evolved which is complementary to these approaches. Plasmonic nanostructures have been shown to have a drastic influence on radiative and non-radiative rate constants [27] (scheme 1(b)), an effect that is generally attributed to changes in the local electric field strength in vicinity of the metal surface [28]. Additionally, the plasmonic nanostructure can also act as an optical antenna on the nanoscale focusing incident excitation light into zeptoliter volumes. When a fluorophore is positioned in such a volume (often referred to as a hotspot) its excitation and emission rates can be enhanced up to several hundred-fold, which allows to enhance its fluorescence signal as well as the photon count rates that can be obtained for single fluorescent molecules. The overall effect of a plasmonic nanostructure on the fluorescence properties of the dye depends on a number of different parameters, such as the distance to the metal surface, the spectral overlap between the excitation and emission spectra of the fluorophore and the plasmon resonance, the size and shape of the plasmonic nanostructure and, in the case of more complex nanoantennas, their spatial arrangement [28–30].

Many studies have focused on the capacity of plasmonic nanoantennas to enhance the fluorescence signal of single emitters, while only a few of them have addressed their unique ability to improve the photostability and the total number of emitted photons [31–34]. Here, the improvement in photostability is typically attributed to an increased radiative rate which, in turn, reduces the time a fluorophore spends in the first excited singlet state and minimizes the probability of photobleaching. In fact, in the simplest approximation where only photobleaching via one photon processes is considered, the total number of photons emitted (N), can be expressed as the ratio of fluorescence quantum yield (Φ_f) and fluorophore bleaching yield (Φ_b) [33, 35]:

$$N = \frac{\Phi_f}{\Phi_b} = \frac{k_r}{k_{all}} \times \frac{k_{all}}{k_b} = \frac{k_r}{k_b} \quad (1)$$

Where, k_r—radiative rate constant, k_b—bleaching rate constant, and k_{all}—sum of all rate constants for photophysical processes occurring from the fluorophore singlet excited state (radiative decay, non-radiative decay, intersystem crossing, and bleaching). Equation (1) illustrates how the photostability of a fluorescent molecule can be improved by either accelerating the radiative rate or decreasing the rate of photobleaching. While traditional photostabilization approaches discussed earlier (scheme 1(a)) are aimed at slowing down the bleaching processes, photostabilization by plasmonic nanostructures (scheme 1(b)) offers an alternative and, perhaps even complementary approach to improve N by accelerating the radiative rate constant. Additionally, the plasmonic nanoparticles have also been shown to increase the radiative and non-radiative decay rates from the triplet excited states also suppressing the time the fluorophore spends in the excited T_1 state (scheme 1(b)) [32, 36, 37]. Depending on the efficiency of this triplet suppression, this offers an additional possibility to further improve the total photon budget (N) of organic fluorophores when coupled to plasmonic nanoantennas.

Plasmonic hotspots formed by a linear arrangement of two metallic nanoparticles exhibit an even greater electric field enhancement [38, 39], with reported values reaching up to 100-fold acceleration of the radiative decay [38]. For a decade now plasmonic dimer nanoantennas have been successfully fabricated via ion or electron beam lithography [40], but this approach suffers from uncontrolled positioning of a fluorophore in the hotspot: usually dyes are either fixed in an aid polymer coating [38] or they are observed as they diffuse freely through the hotspot region [41]. This not only drastically increases the time and the amount of materials spent for a single experiment but creates a large heterogeneity in the enhancement that is achieved for k_{ex} and k_r, as the enhanced electric field varies a lot within a hotspot [42].

Both problems can be addressed by employing an alternative approach of fabricating nanoantennas—self-assembly using DNA origami. In this technique a long single-stranded DNA (ssDNA) with known sequence is shaped with the help of multiple unique ssDNA to a desired configuration [43]. Labelling of a specific strand with a molecule of interest or a functional group (e.g. fluorophore, biotin, amino group) allows to spatially arrange it on a designed structure [44]. This approach has justified itself for performing detailed studies at the single-molecule level of changes in quantum yield and photophysical rates of fluorophores [27], the distance-dependent quenching of fluorescence [45], Förster resonance energy transfer (FRET) [46, 47] and finally, controlled reduction of photobleaching [31, 33] in proximity of metal nanoparticles. These optical antennas have already been employed for single-molecule detection at 25 μM concentration [48] and in diagnostic assays [31, 33, 49]. in proximity of metal nanoparticles.

Nevertheless, the influence of the nanoantenna on the photophysical properties of fluorophores remains to be fully understood. While it is agreed upon that the increase of the radiative decay rates can effectively lead to enhanced quantum yield of fluorophores, their improved photostability, and higher count rates that can be achieved in single-molecule fluorescence studies [31], we discovered that the achievable photon

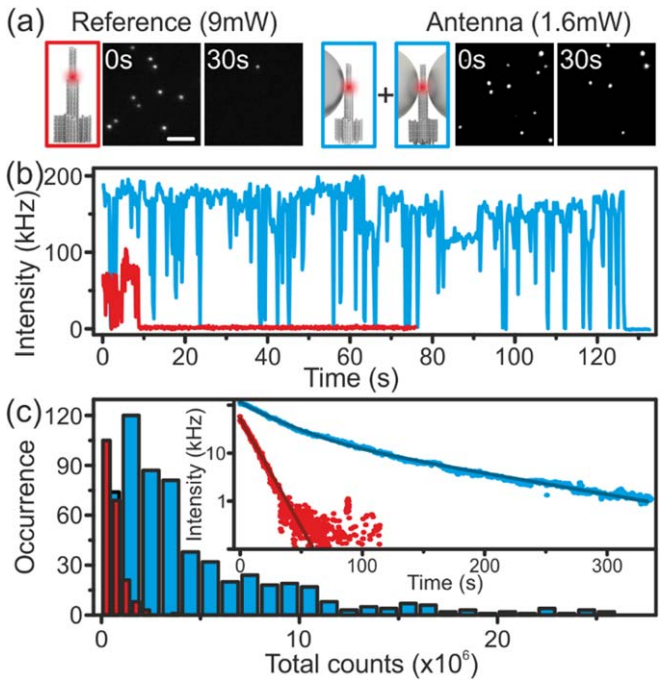

Figure 1. Photostabilization of ATTO 647 N in the hotspot of an Ag DNA nanoantenna. (a) Widefield fluorescence images of ATTO 647 N in the reference (left) and in the nanoantenna (right) samples after 0 s and 30 s of illumination. Scale bar: 10 μm (b) Representative fluorescence intensity versus time trajectories of ATTO 647 N in DNA origami structure (reference, red) and in 100 nm Ag DNA origami nanoantennas (blue) measured at 9 mW and 1.6 mW, respectively; (c) Total number of counts collected from ATTO 647 N in the reference (red) and nanoantenna (blue) samples. 207 and 590 molecules were analyzed for reference and nanoantenna samples, respectively. Inset: average fluorescence intensity over time for the reference (mono-exponential decay fit) and nanoantenna (bi-exponential decay fit) samples.

output of the dye is not only limited by photobleaching but also by other photoinduced processes. By examining the photophysical properties of three dyes (ATTO 542, ATTO 647 N, and AlexaFluor 647) commonly used for single-molecule spectroscopy when placed in the hotspots of dimer 100 nm Ag DNA origami nanoantennas, we demonstrate that despite their improved photostability by the nanoantenna, the maximum photon count rate that can be achieved is still limited by their intrinsic photophysics, such as formation of dim states or increased rate of photoisomerization. Additionally, we show that the enhanced electric field in the hotspot region also poses challenges to the use of non-fluorescent molecules absorbing light, e.g. dark quenchers which are used in fluorescence-based diagnostic assays.

Results and discussion

Improved photon budgets of fluorophores in plasmonic DNA origami nanoantennas

To demonstrate the ability of nanoantennas to even further push the performance and improve the photon budgets of fluorophores in single-molecule fluorescence applications, we performed the photobleaching experiments with one of the most photostable single-molecule dyes—ATTO 647 N. We evaluated the photostability of this dye when placed in the hotspot of a 100 nm Ag DNA origami nanoantenna and compared it to the same dye when placed in the reference DNA origami structure containing no nanoparticles (figure 1(a)). The DNA origami structures were immobilized on BSA-biotin coated glass surfaces via biotin/neutravidin interactions using biotinylated DNA strands on the base of the nanostructure. After this step, the nanoantennas were formed by incorporating DNA functionalized 100 nm Ag nanoparticles. This nanofabrication protocol leads to the mixture of DNA origami structures containing two Ag nanoparticles (dimer) and only one Ag nanoparticle (monomer). The fluorescence intensity of single ATTO 647 N dyes in the nanoantenna and reference structures was monitored over time in a single-molecule wide field microscope in total internal reflection mode. Due to the enhanced local electric field in the nanoantenna hotspot the nanoantenna samples experience higher photon fluxes under the same irradiation intensity. Therefore, in these photobleaching experiments, the nanoantenna samples were excited at 647 nm using a laser power of 1.6 mW, while references samples were excited at a higher laser power of 9 mW [50].

Our single-molecule photobleaching studies demonstrate that even if the photostability of ATTO 647 N is remarkable it can be further improved with the help of a 100 nm Ag nanoantenna without any additional photostabilizers or the need for oxygen removal. Figure 1(a) shows fluorescence images of

ATTO 647 N in the reference and Ag nanoantenna samples acquired at the beginning of the photobleaching experiment (0 s) and after 30 s of illumination. While most of the dyes in the reference sample are photobleached, the fluorescence of ATTO 647 N in the nanoantenna sample is preserved despite the higher fluorescence signal under these excitation powers (see also figure 1(c), inset). Single-molecule fluorescence intensity versus time trajectories were extracted from these photobleaching experiments (see figure 1(b) for exemplary single-molecule trajectories) and the total number of counts until photobleaching was calculated for several hundreds of molecules from the reference and nanoantenna samples. The histograms of total counts detected until photobleaching (figure 1(c)) reveal on average ~10-fold, up to 40-fold for the most efficient nanoantennas improvement in ATTO 647 N photostability when in the hotspot of 100 nm Ag nanoantennas. Here, it is also worth noting that the heterogeneous distribution of total photon counts arises from the heterogeneous fluorescence enhancement and photostabilization efficiencies [39, 51]. The heterogeneous sample composition (monomer and dimer nanoantennas) also results in a bi-exponential photobleaching behavior when compared to the mono-exponential bleaching behavior of the reference sample (figure 1(c), inset).

Based on equation (1) and the radiative rate enhancement estimated by comparing fluorescence intensities normalized by power in nanoantenna samples to reference samples, one would expect a larger improvement in total number of detected photons for ATTO 647 N in the dimer Ag nanoantennas. Previous studies by Pellegrotti *et al* [33]. have shown that at least for monomer Au nanoantennas, the total number of emitted photons by the fluorophore Cy5 was directly proportional to the changes in radiative rate of the fluorophore. However, one also has to consider that due to the electric field enhancement in dimer nanoantennas, fluorophores can experience an order of magnitude higher excitation rates when compared to monomer nanoantennas. Under these excitation conditions higher order photobleaching pathways, such as absorption of a second photon in the S_1 or T_1 states, might become relevant and the approximation made to derive equation (1) might not hold anymore. An indication for this is that no correlation can be seen between fluorescence intensity and total number of emitted photons (See figure S1 is available online at stacks.iop.org/MAF/8/024003/mmedia).

Power saturation and its implications in achieving high count rates required for studying fast dynamics

By providing means to enhance the fluorescence signal and fluorophore photostability, self-assembled DNA nanoantennas hold tremendous promise for advancing single-molecule experiments that require high photon count rates, e.g. studies of single-molecule dynamics that occur on ms to μs time scales. Naively, one would expect that the fluorescence enhancement values provided by nanoantennas directly translate into increased photon count rates. However, by studying the photophysical properties of three common dyes used in single-molecule spectroscopy, e.g. ATTO 542 (rhodamine), ATTO 647 N (carbopyronine), and AlexaFluor 647 (cyanine) when placed in the nanoantenna hotspot, we learned that the picture is more complex. As the dye molecules in the plasmonic hotspot experience a different photophysical environment and much higher photon fluxes, their saturation behavior changes. Figure 2(a) shows the global saturation behavior: in all cases, the onset of saturation is clearly visible for the nanoantenna samples. In the reference samples, however, ATTO 542 and ATTO 647 N show no visible saturation at the same excitation powers, only for AlexaFluor 647 we observe saturation in the reference sample which can be attributed to an accelerated cis-trans isomerization [52] as it will be shown later. Figure 2(b) contains the normalized intensity distribution histograms (per nW of excitation power, calculated by integration of the intensity of a confocal spot) obtained for the three dyes in nanoantenna hotspots. At low excitation powers (100 nW) a wide distribution of intensities is observed assigned to heterogeneous fluorescence enhancement in monomer and dimer nanoantennas. However, as the excitation power is increased (500 nW and 3 μW in figure 2(b)) the distributions become narrower and shift to lower intensities suggesting that the most enhanced and thus the brightest fluorophores are the most sensitive to this saturation behavior.

In contrast to earlier studies on plasmonic enhanced light harvesting complexes [34], we found that this saturation is not originating from any fundamental emission limit of the fluorophore but rather from populating a second emissive state that is less bright in nature. While at low excitation intensities, the formation of this dim state is observed upon longer irradiation times, under increased excitation intensities and, in particular, in the hotspot of nanoantenna where the photon flux is highly increased, these dim states form rather readily. This is illustrated by the single-molecule fluorescence trajectory obtained for ATTO 647 N in the hotspot of a dimer Ag nanoantenna acquired at increasing excitation intensity. Reversible switching between dim and bright states can already be observed at 250 nW, while at 500 nW only the dim state of the dye is visible. A similar photo-induced formation of dim states was observed when analyzing single-molecule trajectories of ATTO 542 and AlexaFluor 647 (see figure S2).

Further mechanistic studies are required to confirm the exact nature of these dim states, however, we propose that it might be related to the formation of spectrally-shifted emissive forms of the fluorophores. Such spectral shifts leading to the formation of blue- and red-shifted emissive forms of fluorophores have

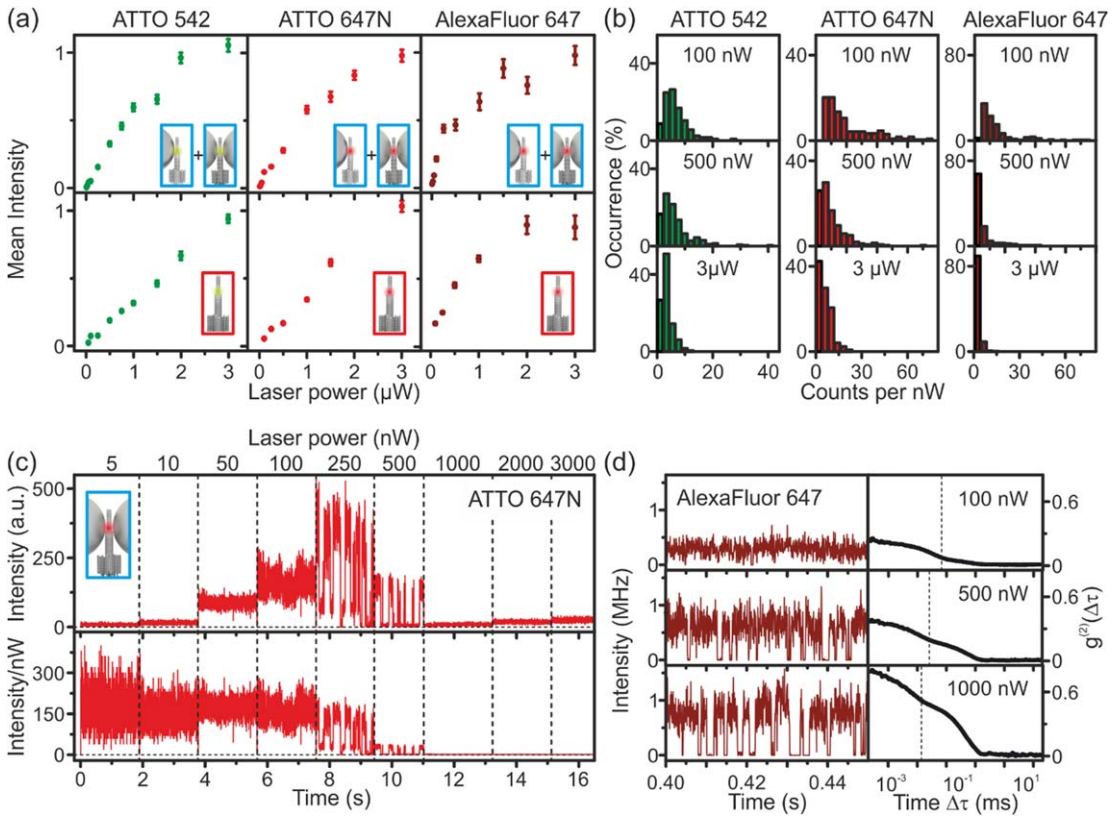

Figure 2. Effect of excitation intensity on the count rates as well as photophysical properties of single ATTO 542 (rhodamine), AlexaFluor 647 (cyanine), and ATTO 647 N (carbopyronine) dyes when placed in the hotspots of plasmonic DNA origami nanoantennas. (a) Power saturation curves obtained for three different dyes from the samples containing 100 nm Ag monomer and dimer nanoantennas. Each data point contains statistics of at least 200 molecules. (b) Intensity distribution histograms normalized per nW of excitation power for the three dyes examined here obtained at three different excitation powers. (c) Top: single-molecule fluorescence trajectory of ATTO 647 N acquired at increasing excitation powers; Bottom: the same single-molecule fluorescence trajectory normalized by excitation power (d) Autocorrelation of the fluorescence signal of an AlexaFluor 647 dye in the nanoantenna measured at different excitation intensities.

previously been observed in single-molecule fluorescence studies of rhodamine [53, 54], oxazine [53], cyanine [53], carbopyronine [5], terrylene diimide [55], and amino-triangulenium [56] dyes. The most extensive mechanistic studies of such spectral instabilities have been carried out for rhodamine class of dyes, where the spectral shift and formation of photo bluing products have been associated with N-dealkylation of tertiary amine groups which proceeds via formation of a radical cation [57, 58]. In this respect, elegant strategies have been developed to overcome these spectral instabilities, e.g. by suppressing the formation of twisted intramolecular charge transfer excited states involved in the N-dealkylation [11, 58–62]. Better understanding of the mechanisms leading to these dim states and development of strategies to mitigate them, combined with the ability of plasmonic nanoantennas to enhance fluorescence signal and photostability, could provide exciting opportunities to push organic fluorophores beyond their current limits.

For the cyanine dye AlexaFluor 647 an additional saturation process is present, which was attributed to photoisomerization from fluorescent *trans* state to a non-fluorescent *cis* state [52, 63]. figure 2(d), shows single-molecule fluorescence trajectories and corresponding autocorrelation curves obtained for AlexaFluor 647 at increasing excitation intensities. The enhanced photoisomerization at increasing excitation intensities is evident from the increase in the amplitude and the rate of the μs-time component. This additional non-radiative relaxation pathway in cyanines together with photoinduced formation of dim states results in a pronounced saturation behavior observed for both reference and nanoantenna samples of AlexaFluor 647 (figure 2(a)). These results suggest that when it comes to achieving high photon count rates, non-rigidified cyanine dyes are not the best fluorophores of choice.

The formation of dim states is the limiting factor in all experiments requiring very high photon count rates, such as single-molecule FRET experiments on fast timescales. Additionally, the power dependence shown in figure 2(a), also implies that one should be cautious when quantifying the fluorescence enhancement values provided by the nanoantenna. As illustrated in figure 2(b), the fluorescence intensity of the dye in the nanoantenna, hence, the calculated fluorescence enhancement, is very sensitive to the excitation intensity chosen for a given experiment. This photoinduced transition to the dark states might also impact

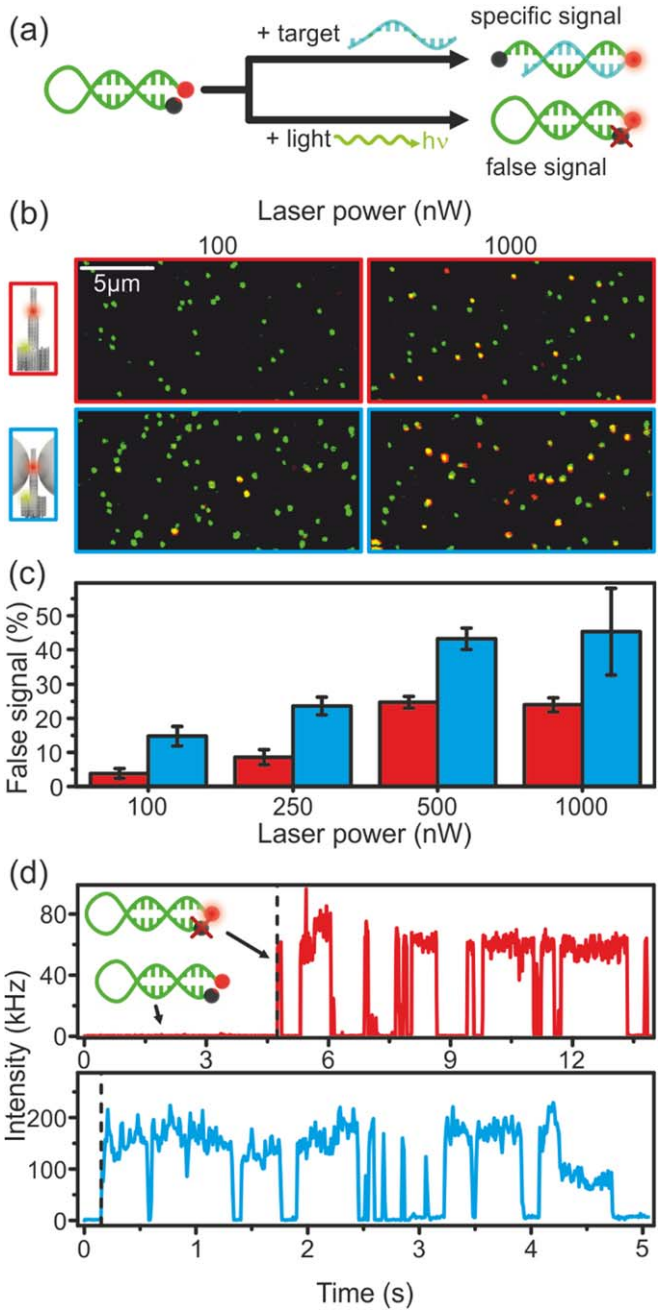

Figure 3. Fluorescence-quenching hairpin (FQH) and accelerated photobleaching of dark quenchers in the hotspot. (a) Schematic representation of FQH construct (for sequence, see SI) bearing ATTO 647 N on the 5′-end and Black Berry Quencher (BBQ650) on the 3′-end. Fluorescence signal from ATTO 647 N ('opened' FQH) is observed either after detection of the target DNA and opening (specific signal) or due to bleaching of BBQ650 (false signal); (b) Confocal fluorescence scans of the DNA origami reference (red) and 100 nm Ag nanoantenna samples bearing an FQH in the hotspot (blue) before addition of the target DNA. Scans are acquired at different powers while exciting with a 639 nm pulsed laser. The DNA origami is labeled with an ATTO 542 dye to allow co-localization of DNA origami and opened FQH. (c) Quantification of the false signal from the confocal fluorescence scans of the DNA origami and DNA origami nanoantennas containing an FQH at different excitation powers, calculated by division of the yellow spots (DNA origami with 'opened' FQH) by the sum of the yellow and green spots (DNA origami with 'closed' FQH). 260 to 440 spots were analyzed for each excitation power. Error bars represent the standard deviation from the mean of the three different scans analyzed. (d) Representative single-molecule trajectories of an FQH illuminated with a 639 nm laser (2 μW for reference (red), 1 μW for nanoantenna (blue)) demonstrating a bleaching event of BBQ650 indicated by the onset of ATTO 647 N fluorescence.

the results of novel biosensing assays in the hotspots of DNA nanoantennas, which rely on a sufficiently high contrast between enhanced and non-enhanced signal. It is therefore of utmost importance to ensure that the dye is emitting from its bright state in order to realize the full potential of plasmonic fluorescence enhancement.

Bleaching of dark quenchers in nanoantenna hotspot and its implications in diagnostics

The modular nature of DNA origami allows the introduction of biorecognition units into the hotspot region of nanoantennas, which offers means to improve the signal-to-noise ratio and overall performance of bioassays. For the successful application of

this concept, it is important to fully understand the photophysical behavior of the reporting unit, which usually consists of one or multiple fluorophores, in the plasmonic hotspot. In our efforts to utilize DNA nanoantennas for diagnostics, we discovered that the performance of diagnostic assays can be significantly influenced by photoinstabilities of dark quenchers when subjected to strong electric fields in the plasmonic hotspot.

Previously, we demonstrated the successful incorporation of a fluorescence-quenching hairpin (FQH) in DNA origami monomer nanoantennas and its application for single-molecule based detection of Zika virus nucleic acids [49]. An FQH, or a molecular beacon, is a self-hybridized nucleic acid sequence containing a fluorescent dye on the one end and a dark quencher on the other end (figure 3(a)). In its closed state, energy transfer from the fluorophore to the quencher occurs due to their close proximity. Upon the detection of the nucleic acid target, which is complementary to a part of the FQH, the hairpin opens increasing the distance between the fluorophore and the quencher and leading to onset of the fluorescence signal (specific signal) [64]. However, we report that photobleaching of the quencher can lead to false positive signal in single-molecule DNA hairpin assays. Due to non-quantitative labelling efficiency and possible photobleaching during handling or measurement steps not every FQH contains a dark quencher. This leads to emission of ATTO 647 N signal (false signal) (figure 3(a)) and therefore decreases the effectiveness of the assay. Although dark quenchers are less likely to take part in different photochemical reactions due to the very short excited state lifetime [65], their photophysics have not been studied under the conditions created in a plasmonic hotspot. Moreover, the effect of these photophysical processes to the bioassay performance has not been assessed.

To perform studies of FQH at the single-molecule level in a hotspot, DNA origami structures were labeled with a green dye (ATTO 542) for initial localization of the construct. The detection efficiency (opening of FQH) in the nanoantenna can be calculated by dividing the number of yellow spots in a fluorescence scan (co-localized signal from ATTO 542 and ATTO 647 N) by the total amount of spots in a fluorescence scan. Even before addition of the target, a small percentage of co-localized spots can be observed due to the reasons mentioned above. Fluorescence scans performed with different excitation powers at 639 nm excitation laser (100 nW—1000 nW) demonstrate an increase in the amount of 'opened' FHQ both for the reference sample (4%–24%) as well as for the 100 nm Ag nanoparticles nanoantenna (15%–45%) (figures 3(b) and (c)). The higher level of false positive signal in the nanoantenna sample can be related to the photobleaching of the dark quencher. From this result it is possible to estimate the quencher survival time knowing the time of exposure for each spot as it is explained in the SI and shown in figure S3. To investigate the photostability of the dark quencher, we illuminated green spots detected in the fluorescence scan with a 639 nm laser at an intensity of 2 μW (reference, red) and 1 μW (nanoantenna, blue). After some time, we observed the occurrence of a signal in the red channel for both, the reference and the nanoantenna sample, which corresponds to the donor fluorescence (figure 3(d)). The reduced quencher survival time is visible in the nanoantenna even at lower excitation power due to the tight focusing of the light. A similar photobleaching behavior has been reported earlier for an ATTO 532/BBQ650 FRET pair [65].

Although the photostability of conventional fluorophores in a plasmonic hotspot is increased [31, 33], the behavior we observed for a fluorophore/quencher reporting unit was very different. In the present study we demonstrated that the dark quencher serving as an energy acceptor in a hotspot can be selectively photobleached in dimer nanoantennas leading to the strong false positive signal and decrease of the overall contrast of the assay.

Conclusion

By using plasmonic nanoantennas, we drastically reduced conventional photobleaching pathways and revealed additional photoinduced processes that limit the maximum photon output of three classes of fluorophores tested here. During our study, we encountered two problems related to the intrinsic photophysics of these dyes: population of weakly fluorescent, dim states - which seems to be a general feature of all tested fluorophores - as well as acceleration of photoisomerization rates at higher excitation powers for cyanine derivatives. Both problems pose a limit on the photon count rates that can be achieved in the plasmonic hotspot. The formation of the dim states could be potentially overcome by utilizing spectrally stable fluorophores [11, 59, 60] The second problem can be circumvented relatively easy by employing fluorophores that do not undergo photoinduced isomerization (e.g. carbopyronines or rhodamines) or by altering the molecular structure of the cyanine dye in order to sterically hinder the isomerization [66].

Here, we also demonstrated that the enhanced excitation rate in the nanoantenna hotspot can affect non-fluorescent chromophores, e.g. dark quenchers. Once placed in a hotspot, the dark quencher experiences not only an efficient energy transfer from the donor dye but also an enhanced electric field and thus an increased excitation rate, which together leads to accelerated photobleaching. This premature photobleaching can be an issue when using fluorogenic probes in a hotspot for different biosensing assays. As illustrated in this work, fast quencher photobleaching can also lead to high false positive signal and decrease

of the overall contrast of the assay. In our case, the photobleaching could be substantially reduced when using lower excitation powers. Alternatively, one could also consider utilizing more stable and robust fluorescence quenchers, such as small gold nanoparticles.

To conclude, we showed that plasmonic hotspots can be employed to substantially enhance the photostability of conventional fluorophores. This enables exciting new applications for fluorescent molecules in which photostability and photon count rate are of crucial importance, such as low-cost single-molecule detectors for point-of-care diagnostics [49], where even the cheapest cameras could potentially be used to detect an infectious disease, or single-molecule biophysics, where the time resolution for FRET experiments could be increased substantially [67]. Here, we show that despite this improved photostability, the performance of conventional dyes used in single-molecule spectroscopy when combined with plasmonic nanoantennas is still limited by their underlying photophysical processes, such as formation of dim states or photoinduced isomerization. We envision that better mechanistic understanding of these limitations and mitigation of the unwanted photophysical pathways, such as the ones described in this work, will contribute to further advancing single-molecule fluorescence applications.

Materials and methods

Fabrication of DNA origami nanoantennas

DNA origami structures were designed in caDNAno2 [68] and assembled and purified using protocols based on Wagenbauer *et al* [69]. In brief, 25 μl of p8064 scaffold (produced in-house) at 100 nM were mixed with 18 μl of unmodified staples pooled from 100 μM original concentration and 2 μl of modified staples, pooled from 100 μM original concentration. All staples were purchased from Eurofins Genomics GmbH (Germany). 5 μl of folding buffer (200 mM $MgCl_2$, 50 mM Tris, 50 mM NaCl, 10 mM EDTA) were added and the mixture was subjected to a thermal annealing ramp (table S1). Samples were purified using 100 kDa MWCO Amicon Ultra filters (Merck, Germany) with 4 washing steps with a lower ionic strength buffer (5 mM $MgCl_2$, 5 mM Tris, 5 mM NaCl, 1 mM EDTA) for 5 min at 10000 rpm, 20 °C.

LabTek-II chambers (Thermo Fisher Scientific, USA) were cleaned with 1 M KOH for at least 20 min, washed three times with PBS buffer and then incubated with BSA-Biotin (0.5 mg mL^{-1}, Sigma-Aldrich, USA) and streptavidin (0.2 mg mL^{-1}, Thermo Fisher Scientific, USA). The origami was immobilized on the biotin-streptavidin surfaces using covalently attached biotin modifications on the six staple strands on the base. Density of DNA origami nanoantennas on the surface suitable for single-molecule measurements was checked on a microscope.

100 nm silver nanoparticles were functionalized with ssDNA based on previously described procedures [49]. 100 nm Silver Nanospheres (Citarate, Biopure) were purchased from nanoComposix (USA). 2 ml nanoparticles (330-fold diluted in MiliQ water) were mixed with 20 μl Tween20 (10%) and 20 μl of a 4:5 (v:v) mixture of 1 M monobasic and dibasic potassium phosphate buffers (Sigma Aldrich, USA) and 20 μl of a 100 μM solution of 3'-thiolated T25 oligonucleotides (Ella Biotech, Germany) and stirred for 1 h at 40 °C. Then, the sodium chloride concentration was subsequently raised to 750 mM using PBS buffer containing 3.3 M NaCl. The solution was centrifuged at 2.8 krcf for 8 min at 20 °C. The supernatant was discarded, and the pellet was re-suspended in PBS containing 10 mM NaCl, 2.11 mM P8709 buffer (Sigma Aldrich, USA), 2.89 mM P8584 buffer (Sigma Aldrich, USA), 0.01% Tween20 and 1 mM EDTA. This washing step was repeated five times. Then, the pellet was re-suspended in TE buffer containing 750 mM NaCl and the concentration was adjusted to reach 0.1 absorption at 485 nm (maximum of absorbance) on a UV–vis spectrometer (Nanodrop 2000, Thermo Fisher Scientific, USA). To bind the nanoparticles to the origami, the chambers were incubated with 100 μl of this solution overnight.

Confocal microscopy

Confocal fluorescence measurements were performed using a home-built confocal setup based on an Olympus IX-83 inverted microscope (Japan) and a 78 MHz-pulsed supercontinuum white light laser (SuperK Extreme, NKT Photonics, Denmark) with selected wavelengths of 532 nm and 639 nm. The wavelengths are selected via an acousto-optically tunable filter (AOTF, SuperK Dual AOTF, NKT Photonics, Denmark). This is controlled by a digital controller (AODS 20160 8 R, Crystal Technology, USA) via a computer software (AODS 20160 Control Panel, Crystal Technology, USA). A second AOTF (AA.AOTF.ns: TN, AA Opto-Electronic, France) was be used to alternate 532 nm and 639 nm wavelengths if required, as well as to further spectrally clean the laser beam. It is controlled via home-made LabVIEW software (National Instruments, USA). A neutral density filter was used to regulate the laser intensity, followed by a linear polarizer and a $\lambda/4$ plate to achieve circularly polarized excitation. A dichroic beam splitter (ZT532/640rpc, Chroma, USA) and an immersion oil objective (UPlanSApo 100×, NA = 1.4, WD = 0.12 mm, Olympus, Japan) were used to focus the excitation laser onto the sample. Micropositioning was performed using a Piezo-Stage (P-517.3CL, E-501.00, Physik Instrumente GmbH&Co. KG, Germany). Emitted light was then collected using the same

objective and filtered from the excitation light by the dichroic beam splitter. The light was later focused on a 50 μm pinhole (Linos) and detected using Single-Photon Avalanche Diodes (SPCM, AQR 14, PerkinElmer, USA) registered by an TCSPC system (HydraHarp 400, PicoQuant, Germany) after additional spectral filtering (RazorEdge 647, Semrock, USA for a red channel and HC582/75, AHF Analysentechnik, Germany for a green channel). A custom-made LabVIEW software (National Instruments, USA) was used to process the acquired raw data. The autocorrelation of the Alexa Fluor 647 signal was calculated using SymphoTime 64 (PicoQuant, Germany). For the fluorescence autocorrelation, measurements were carried out in a reducing and oxidizing buffer system with enzymatic oxygen removal consisting of 90% buffer a (100 mM $MgCl_2$, 40 mM Tris, 2 mM Trolox/Troloxquinone and 1% w/v Glucose) and 10% buffer b (glucose oxidase (1 mg ml^{-1}), 0.4% (v/v) catalase (50 μg ml^{-1}), 30% glycerol, 12.5 mM KCl in 50 mM TRIS).

Photostability studies on the wide-field microscope

Single-molecule photostability studies of nanoantenna and the reference samples were performed on the commercial Nanoimager S (ONI, UK). Samples were illuminated with a 640-nm laser at 53.5° angle to achieve evanescent excitation due to total internal reflection at the glass-water interface. Reference samples were excited with laser power of 9 mW, while nanoantenna samples where imaged at 1.6 mW. The laser beam was focused onto the back-focal plane of an oil-immersion objective (100×, NA = 1.4) and the emission light was detected with an sCMOS camera. Simultaneous photobleaching of few hundreds of fluorescent molecules was recorded in the field of view of 50 × 80 μm. For further analysis, only the central region with even illumination was used. Single-molecule fluorescence intensity versus time trajectories were extracted using a home-built analysis routine in ImageJ. The intensity of a circular regions of 8 pixels in diameter around the molecules were integrated as a function of time. For the background correction from these transients the average intensity of at least 15 regions of the 8-pixel areas containing no molecules was subtracted. To get the total counts from molecules the sum of intensity after the background subtraction was calculated.

Acknowledgments

We gratefully acknowledge financial support from the DFG (INST 86/1904-1 FUGG, excellence clusters NIM and e-conversion), BMBF (Grants POCEMON, 13N14336, and SIBOF, 03VP03891), and the European Union's Horizon 2020 research and innovation program under grant agreement No. 737089 (Chipscope). V G and K T acknowledge the support by Humboldt Research Fellowship from the Alexander von Humboldt Foundation. The authors have declared that no conflicting interests exist.

ORCID iDs

Lennart Grabenhorst https://orcid.org/0000-0001-9503-1819
Florian Steiner https://orcid.org/0000-0002-9148-5837
Viktorija Glembockyte https://orcid.org/0000-0003-2531-6506
Philip Tinnefeld https://orcid.org/0000-0003-4290-7770

References

[1] Ha T and Tinnefeld P 2012 Photophysics of fluorescent probes for single-molecule biophysics and super-resolution imaging *Annu. Rev. Phys. Chem.* **63** 595–617
[2] Nettels D, Gopich I V, Hoffmann A and Schuler B 2007 Ultrafast dynamics of protein collapse from single-molecule photon statistics *Proc. Natl Acad. Sci. USA* **104** 2655–60
[3] Chung H S, McHale K, Louis J M and Eaton W A 2012 Single-molecule fluorescence experiments determine protein folding transition path times *Science* **335** 981–4
[4] Cordes T, Vogelsang J and Tinnefeld P 2009 On the mechanism of trolox as antiblinking and antibleaching reagent *J. Am. Chem. Soc.* **131** 5018–9
[5] Vogelsang J, Kasper R, Steinhauer C, Person B, Heilemann M, Sauer M and Tinnefeld P 2008 A reducing and oxidizing system minimizes photobleaching and blinking of fluorescent dyes *Ang. Chem. Int. Ed.* **47** 5465–9
[6] Rasnik I, McKinney S A and Ha T 2006 Nonblinking and long-lasting single-molecule fluorescence imaging *Nat. Meth.* **3** 891–3
[7] Glembockyte V, Lin J and Cosa G 2016 Improving the photostability of red- and green-emissive single-molecule fluorophores via Ni^{2+} mediated excited triplet-state quenching *J. Phys. Chem.* B **120** 11923–9
[8] Dave R, Terry D S, Munro J B and Blanchard S C 2009 Mitigating unwanted photophysical processes for improved single-molecule fluorescence imaging *Biophys. J.* **96** 2371–81
[9] Gust A, Zander A, Gietl A, Holzmeister P, Schulz S, Lalkens B, Tinnefeld P and Grohmann D 2014 A starting point for fluorescence-based single-molecule measurements in biomolecular research *Molecules* **19** 15824
[10] Cordes T, Maiser A, Steinhauer C, Schermelleh L and Tinnefeld P 2011 Mechanisms and advancement of antifading agents for fluorescence microscopy and single-molecule spectroscopy *Phys. Chem. Chem. Phys.* **13** 6699–709
[11] Grimm J B *et al* 2016 Bright photoactivatable fluorophores for single-molecule imaging *Nat. Methods* **13** 985–8
[12] Zheng Q and Lavis L D 2017 Development of photostable fluorophores for molecular imaging *Curr. Opin. Struct. Biol.* **39** 32–8
[13] Stennett E M S, Ciuba M A and Levitus M 2014 Photophysical processes in single molecule organic fluorescent probes *Chem. Soc. Rev.* **43** 1057–75
[14] Widengren J, Chmyrov A, Eggeling C, Löfdahl P-Å and Seidel C A M 2006 Strategies to improve photostabilities in ultrasensitive fluorescence spectroscopy *J. Phys. Chem.* A **111** 429–40
[15] Glembockyte V, Lincoln R and Cosa G 2015 Cy3 photoprotection mediated by Ni^{2+} for extended single-

molecule imaging: old tricks for new techniques *J. Am. Chem. Soc.* **137** 1116–22
[16] Glembockyte V, Wieneke R, Gatterdam K, Gidi Y, Tampé R and Cosa G 2018 Tris-N-nitrilotriacetic acid fluorophore as a self-healing dye for single-molecule fluorescence imaging *J. Am. Chem. Soc.* **140** 11006–12
[17] Holzmeister P, Gietl A and Tinnefeld P 2014 Geminate recombination as a photoprotection mechanism for fluorescent dyes *Ang. Chem. Int. Ed.* **53** 5685–8
[18] Glembockyte V and Cosa G 2017 Redox-based photostabilizing agents in fluorescence imaging: the hidden role of intersystem crossing in geminate radical ion pairs *J. Am. Chem. Soc.* **139** 13227–33
[19] Tinnefeld P and Cordes T 2012 'Self-healing' dyes: intramolecular stabilization of organic fluorophores *Nat. Meth.* **9** 426–7
[20] Altman R B, Terry D S, Zhou Z, Zheng Q, Geggier P, Kolster R A, Zhao Y, Javitch J A, Warren J D and Blanchard S C 2012 Cyanine fluorophore derivatives with enhanced photostability *Nat. Meth.* **9** 68–71
[21] van der Velde J H M *et al* 2016 A simple and versatile design concept for fluorophore derivatives with intramolecular photostabilization *Nat. Commun.* **7** 10144
[22] van der Velde J H M, Oelerich J, Huang J, Smit J H, Hiermaier M, Ploetz E, Herrmann A, Roelfes G and Cordes T 2014 The power of two: covalent coupling of photostabilizers for fluorescence applications *J. Phys. Chem. Lett.* **5** 3792–8
[23] van der Velde J H M, Ploetz E, Hiermaier M, Oelerich J, de Vries J W, Roelfes G and Cordes T 2013 Mechanism of intramolecular photostabilization in self-healing cyanine fluorophores *Chem. Phys. Chem.* **14** 4084–93
[24] Zheng Q, Jockusch S, Zhou Z, Altman R B, Warren J D, Turro N J and Blanchard S C 2012 On the mechanisms of cyanine fluorophore photostabilization *J. Phys. Chem. Lett.* **3** 2200–3
[25] van der Velde J H M, Uusitalo J J, Ugen L-J, Warszawik E M, Herrmann A, Marrink S J and Cordes T 2015 Intramolecular photostabilization via triplet-state quenching: design principles to make organic fluorophores 'self-healing' *Farad. Discuss.* **184** 221–35
[26] Smit J H, van der Velde J H M, Huang J, Trauschke V, Henrikus S S, Chen S, Eleftheriadis N, Warszawik E M, Herrmann A and Cordes T 2019 On the impact of competing intra- and intermolecular triplet-state quenching on photobleaching and photoswitching kinetics of organic fluorophores *Phys. Chem. Chem. Phys.* **21** 3721–33
[27] Holzmeister P, Pibiri E, Schmied J J, Sen T, Acuna G P and Tinnefeld P 2014 Quantum yield and excitation rate of single molecules close to metallic nanostructures *Nat. Commun.* **5** 5356
[28] Anger P, Bharadwaj P and Novotny L 2006 Enhancement and quenching of single-molecule fluorescence *Phys. Rev. Lett.* **96** 113002
[29] Heck C, Prinz J, Dathe A, Merk V, Stranik O, Fritzsche W, Kneipp J and Bald I 2017 Gold nanolenses self-assembled by DNA origami *ACS Photonics* **4** 1123–30
[30] Maier S A 2007 *Plasmonics: Fundamentals and Applications.* (United States of America: Springer Science & Business Media)
[31] Kaminska I, Vietz C, Cuartero-González Á, Tinnefeld P, Fernández-Domínguez A I and Acuna G P 2018 Strong plasmonic enhancement of single molecule photostability in silver dimer optical antennas *Nanophotonics* **7** 643–9
[32] Kéna-Cohen S, Wiener A, Sivan Y, Stavrinou P N, Bradley D D C, Horsfield A and Maier S A 2011 Plasmonic sinks for the selective removal of long-lived states *ACS Nano* **5** 9958–65
[33] Pellegrotti J V, Acuna G P, Puchkova A, Holzmeister P, Gietl A, Lalkens B, Stefani F D and Tinnefeld P 2014 Controlled reduction of photobleaching in DNA origami–gold nanoparticle hybrids *Nano Lett.* **14** 2831–6
[34] Wientjes E, Renger J, Cogdell R and van Hulst N F 2016 Pushing the photon limit: nanoantennas increase maximal photon stream and total photon number *J. Phys. Chem. Lett.* **7** 1604–9
[35] Hirschfeld T 1976 Quantum efficiency independence of the time integrated emission from a fluorescent molecule *Appl. Opt.* **15** 3135–9
[36] Zhang Y, Aslan K, Previte M J R, Malyn S N and Geddes C D 2006 Metal-enhanced phosphorescence: interpretation in terms of triplet-coupled radiating plasmons *J. Phys. Chem.* B **110** 25108–14
[37] Pacioni N L, González-Béjar M, Alarcón E, McGilvray K L and Scaiano J C 2010 Surface plasmons control the dynamics of excited triplet states in the presence of gold nanoparticles *J. Am. Chem. Soc.* **132** 6298–9
[38] Kinkhabwala A, Yu Z, Fan S, Avlasevich Y, Müllen K and Moerner W E 2009 Large single-molecule fluorescence enhancements produced by a bowtie nanoantenna *Nat. Photonics* **3** 654–7
[39] Acuna G P, Moller F M, Holzmeister P, Beater S, Lalkens B and Tinnefeld P 2012 Fluorescence enhancement at docking sites of DNA-directed self-assembled nanoantennas *Science* **338** 506–10
[40] Sundaramurthy A, Schuck P J, Conley N R, Fromm D P, Kino G S and Moerner W E 2006 Toward nanometer-scale optical photolithography: utilizing the near-field of bowtie optical nanoantennas *Nano Lett.* **6** 355–60
[41] Punj D, Mivelle M, Moparthi S B, van Zanten T S, Rigneault H, van Hulst N F, Garcia-Parajo M F and Wenger J 2013 A plasmonic 'antenna-in-box' platform for enhanced single-molecule analysis at micromolar concentrations *Nat. Nanotechnol.* **8** 512–6
[42] Chikkaraddy R *et al* 2018 Mapping nanoscale hotspots with single-molecule emitters assembled into plasmonic nanocavities using DNA origami *Nano Lett.* **18** 405–11
[43] Rothemund P W K 2006 Folding DNA to create nanoscale shapes and patterns *Nature* **440** 297–302
[44] Schreiber R, Do J, Roller E-M, Zhang T, Schüller V J, Nickels P C, Feldmann J and Liedl T 2013 Hierarchical assembly of metal nanoparticles, quantum dots and organic dyes using DNA origami scaffolds *Nat. Nanotechnol.* **9** 74
[45] Acuna G P *et al* 2012 Distance dependence of single-fluorophore quenching by gold nanoparticles studied on DNA origami *ACS Nano* **6** 3189–95
[46] Aissaoui N, Moth-Poulsen K, Käll M, Johansson P, Wilhelmsson L M and Albinsson B 2017 FRET enhancement close to gold nanoparticles positioned in DNA origami constructs *Nanoscale* **9** 673–83
[47] Bohlen J, Cuartero-González Á, Pibiri E, Ruhlandt D, Fernández-Domínguez A I, Tinnefeld P and Acuna G P 2019 Plasmon-assisted Förster resonance energy transfer at the single-molecule level in the moderate quenching regime *Nanoscale* **11** 7674–81
[48] Puchkova A, Vietz C, Pibiri E, Wunsch B, Sanz Paz M, Acuna G P and Tinnefeld P 2015 DNA origami nanoantennas with over 5000-fold fluorescence enhancement and single-molecule detection at 25 muM *Nano Lett.* **15** 8354–9
[49] Ochmann S E, Vietz C, Trofymchuk K, Acuna G P, Lalkens B and Tinnefeld P 2017 Optical nanoantenna for single molecule-based detection of zika virus nucleic acids without molecular multiplication *Anal. Chem.* **89** 13000–7
[50] We note that decreasing the power at which we excite the reference would have prevented us from detecting every molecule, while increasing the power at which we excite the nanoantenna sample would have led to saturation effects
[51] Vietz C, Kaminska I, Sanz Paz M, Tinnefeld P and Acuna G P 2017 Broadband fluorescence enhancement with self-assembled silver nanoparticle optical antennas *ACS Nano* **11** 4969–75
[52] Widengren J and Schwille P 2000 Characterization of photoinduced isomerization and back-isomerization of the cyanine dye Cy5 by fluorescence correlation spectroscopy *J. Phys. Chem.* A **104** 6416–28
[53] Tinnefeld P, Herten D-P and Sauer M 2001 Photophysical dynamics of single molecules studied by spectrally-resolved

fluorescence lifetime imaging microscopy (SFLIM) *J. Phys. Chem.* A **105** 7989–8003
[54] Heilemann M, Tinnefeld P, Sanchez Mosteiro G, Garcia Parajo M, Van Hulst N F and Sauer M 2004 Multistep energy transfer in single molecular photonic wires *JACS* **126** 6514–5
[55] Liao Z, Hooley E N, Chen L, Stappert S, Müllen K and Vosch T 2013 Green emitting photoproducts from terrylene diimide after red illumination *JACS* **135** 19180–5
[56] Liao Z, Bogh S A, Santella M, Rein C, Sørensen T J, Laursen B W and Vosch T 2016 Emissive photoconversion products of an amino-triangulenium dye *J. Phys. Chem.* A **120** 3554–61
[57] Evans N A 1973 Photofading of rhodamine dyes: II. Photodealkylation of rhodamine B *J. Soc. Dyers Colour.* **89** 332
[58] Butkevich A N, Bossi M L, Lukinavicius G and Hell S W 2019 Triarylmethane fluorophores resistant to oxidative photobluing *J. Am. Chem. Soc.* **141** 981–9
[59] Song X, Johnson A and Foley J 2008 7-Azabicyclo[2.2.1] heptane as a unique and effective dialkylamino auxochrome moiety: demonstration in a fluorescent rhodamine dye *JACS* **130** 17652–3
[60] Liu X, Qiao Q, Tian W, Liu W, Chen J, Lang M J and Xu Z 2016 Aziridinyl fluorophores demonstrate bright fluorescence and superior photostability by effectively inhibiting twisted intramolecular charge transfer *JACS* **138** 6960–3
[61] Grimm J B *et al* 2015 A general method to improve fluorophores for live-cell and single-molecule microscopy *Nat. Methods* **12** 244–50
[62] Grimm J B *et al* 2017 A general method to fine-tune fluorophores for live-cell and *in vivo* imaging *Nat. Methods* **14** 987–94
[63] Levitus M and Ranjit S 2011 Cyanine dyes in biophysical research: the photophysics of polymethine fluorescent dyes in biomolecular environments *Q. Rev. Biophys.* **44** 123–51
[64] Tyagi S and Kramer F R 1996 Molecular beacons: probes that fluoresce upon hybridization *Nat. Biotechnol.* **14** 303–8
[65] Holzmeister P, Wunsch B, Gietl A and Tinnefeld P 2014 Single-molecule photophysics of dark quenchers as non-fluorescent FRET acceptors *Photochem. Photobiol. Sci.* **13** 853–8
[66] Michie M S, Gotz R, Franke C, Bowler M, Kumari N, Magidson V, Levitus M, Loncarek J, Sauer M and Schnermann M J 2017 Cyanine conformational restraint in the far-red range *J. Am. Chem. Soc.* **139** 12406–9
[67] Chung H S and Eaton W A 2018 Protein folding transition path times from single molecule FRET *Curr. Opin. Struct. Biol.* **48** 30–9
[68] Douglas S M, Marblestone A H, Teerapittayanon S, Vazquez A, Church G M and Shih W M 2009 Rapid prototyping of 3D DNA-origami shapes with caDNAno *Nucleic Acids Res.* **37** 5001–6
[69] Wagenbauer K F, Engelhardt F A S, Stahl E, Hechtl V K, Stommer P, Seebacher F, Meregalli L, Ketterer P, Gerling T and Dietz H 2017 How we make DNA origami *Chem. Bio. Chem.* **18** 1873–85